ACS APPLIED MATERIALS & INTERFACES

Research Article

www.acsami.org

Inkjet Printing of Silver Nanowire Networks

David J. Finn, Mustafa Lotya, and Jonathan N. Coleman*

School of Physics, Centre for Research on Adaptive Nanostructures and Nanodevices (CRANN), and Advanced Materials and Bio-Engineering Research (AMBER), Trinity College Dublin, Dublin 2, Ireland

Supporting Information

ABSTRACT: The development of printed electronics will require the ability to deposit a wide range of nanomaterials using printing techniques. Here we demonstrate the controlled deposition of networks of silver nanowires in well-defined patterns by inkjet printing from an optimized isopropyl alcohol−diethylene glycol dispersion. We find that great care must be taken while producing the ink and during solvent evaporation. The resultant networks have good electrical properties, displaying sheet resistances as low as 8 Ω/□ and conductivities as high as 10^5 S/m. Such optimized performances were achieved for line widths of 1−10 mm and network thicknesses of 0.5−2 μm deposited from ∼10−20 passes while using processing temperatures of no more than 110 °C. Thin networks are semitransparent with dc to optical conductivity ratios of ∼40.

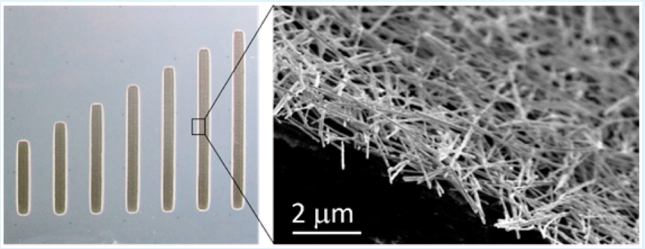

KEYWORDS: *printed electronics, solution processing, nanomaterials, network, percolation, silver nanowires, silver nanoink, inkjet fabrication of Ag nanowires*

1. INTRODUCTION

The production of low-cost electronic devices will be revolutionized by the ability to print functional materials. Printed electronics involves the additive fabrication of devices on substrates and over large areas at relatively low temperatures. One of the simplest methods is inkjet printing, a noncontact, additive process which can deposit droplets of ink on a substrate in predefined patterns.[1] Devices can be inkjet printed from any material that can be dispersed, suspended, or dissolved in a liquid. Examples of advanced materials which have been printed in this way[2] are polymers/nanocomposites,[3−6] nanoparticles,[7,8] carbon nanotubes,[9−15] graphene,[16−27] and most recently MoS_2 nanosheets.[26,28−30] These materials have been used to fabricate a range of devices including photodetectors,[26] transistors,[30−32] sensors,[5,33,34] light-emitting diodes,[35] supercapacitors,[36,37] and solar cells.[4,38]

One important application of inkjet printing is the fabrication of conductive elements in printed circuitry. While poly[3,4-(ethylenedioxy)thiophene] (PEDOT)/poly(styrenesulfonate) (PSS),[39] carbon nanotubes,[13,40] and graphene nanosheets[16−26] have been proposed for use in this space, probably the most successful conductive inks have been based on metallic nanoparticles[10,41−45] (see the Supporting Information for a literature review table). Inkjet printing of metallic nanoparticles can result in conductive traces with conductivity approaching that of bulk metal.[14] However, achieving such high conductivities generally requires annealing, which can be problematic when working with polymeric substrates. In addition, the annealed structures tend to be dense and therefore highly optically absorbing. This makes metallic nanoparticles unsuited for printed applications where transparency is required.[46]

Conversely, metallic nanowires, most commonly found as silver nanowires (AgNWs), have recently demonstrated huge potential in transparent electrode applications.[46,47] Highly conductive silver nanowire electrodes can be fabricated at low temperature and over large areas and are extremely flexible.[48−50] They have demonstrated sheet resistances as low as 5 Ω/□ for transparencies of 90%.[50] However, while many methods for the deposition of metallic nanowires have been investigated,[48,49,51−55] direct writing of patterned, high-quality silver nanowire networks has proven extremely difficult. To the best of the our knowledge, very few papers have described direct writing of metallic nanowire traces, in this case using inkjet printing.[56−58] Of the papers that do exist, only one describes the printing of AgNWs in any detail.[57] This paper described the printing of AgNWs as a minority component in a AgNW/silver nitrate mixture. The printed structures were converted to silver lines by annealing at 200 °C. While this work is of great interest, we believe it is important to demonstrate and describe the inkjet printing of structures consisting solely of silver nanowires, preferably at temperatures which are low enough to be compatible with plastic substrates. This is extremely challenging as the high aspect ratio of silver nanowires makes it extremely difficult to print without blocking of the jetting nozzles. In addition, the high density of silver means a given suspended nanowire mass fraction is equivalent

Received: March 2, 2015
Accepted: April 15, 2015
Published: April 15, 2015

DOI: 10.1021/acsami.5b01875
ACS Appl. Mater. Interfaces 2015, 7, 9254−9261

to a very low volume fraction. This results in a relatively small number of wires deposited per volume of liquid printed, leading to difficulties with solvent management.

We believe the ability to print patterned networks of silver nanowires is important as it would allow the fabrication of patterned, flexible structures which are extremely conductive and highly transparent. Critically, this should be achievable at low temperatures, making this method suitable for use with plastic substrates. In this work, we demonstrate inkjet printing of silver nanowire networks on flexible substrates. We outline both the problems and the solutions which must be found to achieve successful printing. We characterize the resulting networks electrically and show them to be promising for use in printed conducting applications.

2. RESULTS AND DISCUSSION

2.1. Printing Silver Nanowires. Before conductive patterns of AgNWs on flexible substrates such as poly(ethylene terephthalate) (PET) are printed, a number of significant problems must be resolved. For example, the as-delivered nanowires must be shortened and the concentration optimized to avoid nozzle congestion while the correct solvent mixture with appropriate rheological properties must be identified to ensure good jetting performance. The combination of drying procedure and required number of print passes must be carefully managed, while an appropiate post-printing annealing procedure, which is compatible with the polymeric substrate, must be developed to obtain conducting networks. We note that detailed information outlining our efforts to resolve these issues is given in the Supporting Information.

The silver nanowires used in this work were purchased from Seashell Technology as a suspension in isopropyl alcohol (IPA; 5 mg/mL). These wires are coated with a proprietary organic stabilizing agent which prevents aggregation of the wires in isopropyl alcohol. As a result, all experiments used isopropyl alcohol as the main solvent. Scanning electron microscopy showed the suspended nanowires to have an average diameter of 55 nm and an average length of 8.1 μm. These wires are relatively rigid and show no entanglement and very little bending. In this work, a Dimatix materials printer (16 nozzle printhead, nozzle diameter a = 21.5 μm). It is well-known that printing of nanomaterials generally works best when the nano-object's long dimension is less than a/50. However, we reasoned that this criterion might not be as stringent for nanowires due to the possibility of flow-induced alignment as the wires passed through the nozzles. We reduced the nanowire length to 2.2 μm by sonication-induced scission[59] in a low-power ultrasonic bath for 3 h. Trials showed that, even though the length of these wires was larger than a/50, they could indeed be successfully inkjetted (see the Supporting Information for more details).

However, nanowires dispersed in isopropyl alcohol alone do not inkjet well mainly because the solution viscosity is too low. This manifests itself in the formation of satellite droplets and generally poor printing. We found that dilution of the isopropyl alcohol suspension and the addition of diethylene glycol (DEG), such that the total nanowire concentration was 0.85 mg/mL and the IPA:DEG volumetric ratio was 0.85:0.15, gave the best printing performance without the production of any satellite droplets. We note that compositions of 0.90:0.10 and 0.80:0.20 did not print well (see the Supporting Information for more details). We measured the room temperature viscosity and surface tension of this optimized suspension to be η = 4.6 $\pm$ 0.3 mPa s and γ = 28 mJ/m^2 using an Anton-Paar MCR 301 rheometer (parallel plate PP50 geometry) and a TBS torsion balance, model OS, respectively. This results in an inverse Ohnesorge number,[60] $Z = (\gamma\rho a)^{1/2}/\eta \approx 4.7$ ($\rho \approx 800$ kg/m^3 is the liquid density), well within the accepted range for inkjet printing: $1 < Z < 14$.[25] The nonoptimized compositions (0.90:0.10 and 0.80:0.20) had Z values approximately 25% above and below the optimized composition, respectively. We note that the nanowire suspension was heated to 40 °C within the actuation chamber to facilitate subsequent drying. However, the resultant reduction in η is certainly not enough to shift Z out of the required range. Interestingly, we found that if the concentration was increased above 1 mg/mL, printing was impossible due to rapid clogging of the nozzles (see the Supporting Information for more details).

A significant problem is controlling solvent evaporation during and after deposition. Because of the high density of silver, the solids volume fraction at the optimized concentration (0.85 mg/mL) is considerably lower than would be the case for a low-density material such as graphene. As such, for a given volume of nanowires deposited on a surface, the solvent volume which must be removed is proportionally larger. To evaporate the solvent, we initially tried heating the substrate on a vacuum platen at 60 °C during and after printing. However, we found that this resulted in insulating networks, perhaps due to removal of the organic coating, leading to nanowire oxidation in the heated liquid. To address this, we reduced the platen temperature to 40 °C, achieving reasonable solvent evaporation (see the Supporting Information for more details). However, to increase the network thickness, it is necessary to increase the number of print passes, N. We found that, for more than 10 print passes, solvent tended to bleed out from the printed lines, flooding the substrate. This resulted in very poor quality, nonuniform printed lines.

We found we could address this problem by introducing an intermediate drying step during a print session (see the Supporting Information for more details). After 10 print passes, the printed PET substrate was placed into a vacuum oven at a temperature of 110 °C and pumped down to a pressure of 0.1 mPa for 30 min to slowly evaporate the solvent. In the next step, the substrate was taken out of the oven and realigned on the printer platen. The printing session was resumed with subsequent printing on top of the oven-dried traces. This process was repeated every 10 passes and largely eliminated the bleeding of the solvent vehicle for print runs with a large number of passes. After completion of the printing session, the inkjet-printed substrate was placed again in the oven under vacuum and annealed at 110 °C for a period not exceeding 2 h. We note that this final drying step also acted as an annealing step to decrease the interjunction resistivity of the overlapping nanowires and increase the dc conductivity of the network.[52]

In this way it is possible to print good quality line features and patterns from silver nanowires as shown in Figure 1A. It is very easy to control the lateral dimensions of the features, for example the length and width of the printed lines (Figure 1B). As indicated above, the thickness of the printed features can be controlled via the number of print passes, N. We investigate the uniformity of such printed features using scanning electron microscopy. Shown in Figure 1C is an scanning electron microscopy (SEM) image of a relatively thin silver nanowire network (N = 12), which demonstrates the uniformity of these printed features. Figure 1D shows an image of a thicker network (N = 80) focusing on the edge region. This image

DOI: 10.1021/acsami.5b01875
ACS Appl. Mater. Interfaces 2015, 7, 9254−9261

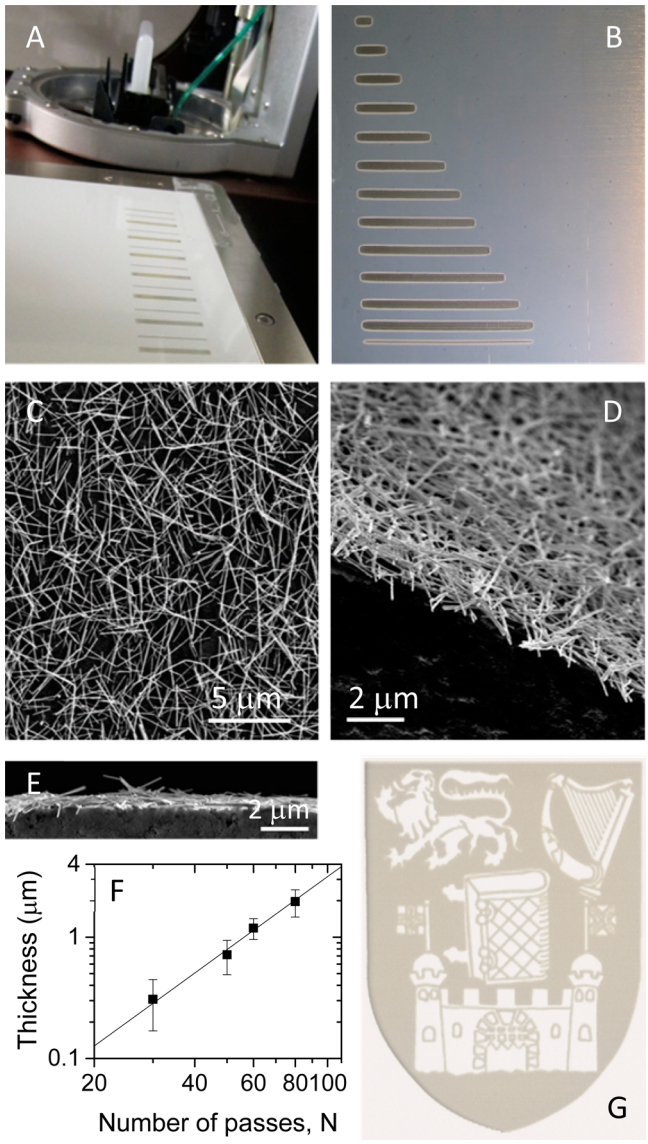

Figure 1. Inkjet-printed silver nanowire networks. (A) Inkjet printing of silver nanowire lines on a coated PET substrate which has been aligned with index pins on the printer's heated platen. (B) Printed lines of different lengths (w = 2 mm, N = 20). (C) SEM image of a relatively thin silver nanowire network (N = 12 passes). (D, E) SEM images of the edges of thick nanowire networks (D, N = 80 passes; E, N = 50 passes). (F) Network thickness, as measured by SEM, as a function of the number of passes. (G) Inkjet-printed nanowire network in the shape of the Trinity College Dublin crest. The width of this crest is ∼4 cm.

highlights that these networks consist of largely random arrays of rigid AgNWs. By examining freeze-fractured nanowire networks edge-on (Figure 1E), it is possible to estimate the network thickness. We performed this analysis for a number of networks prepared with different numbers of print passes. As shown in Figure 1F, the measured thickness clearly scales with N. However, unlike the linear behavior previously observed for inkjet-printed graphene networks,[22,26] here we observe the network thickness to scale very clearly with the square of the number of passes. Fitting these data gives the relationship

$$t\ (\mathrm{nm}) = 3.16N^{1.95\pm0.16} \quad (1)$$

which allows us to estimate the thickness for a given number of passes assuming the suspension concentration and printing conditions remain constant. It is not clear why this relationship should be superlinear; however, we suggest it may be related to the issues associated with solving drying described above.

Once this process optimization has been achieved, it is possible to directly deposit patterned networks. To demonstrate this, we printed out the Trinity College Dublin crest as shown in Figure 1G. It is clear from this image that the accuracy and resolution achievable using this process is reasonably good, at least at length scales above ∼100 μm (see below).

2.2. Network Uniformity. To further assess the thickness uniformity of the printed AgNW networks, we performed transmission scanning[48] on a network produced with N = 20 and w = 2 mm. In this method, the local transmittance of the sample is measured with a pixel size of ∼6 μm. Scanning was performed on the network deposited on a PET substrate. The resultant transmittance measurements can then be plotted as a map to form an image such as the one shown in Figure 2A. In this image, the printed line is clearly apparent. It can be seen that the edge of the line is somewhat rough, with a line-edge roughness of 100−200 μm. In addition, horizontal striations can be seen in the print pattern which are aligned in the raster direction (x-axis). These are known as swathe edges in the printing industry and occur along the direction parallel to the ink head raster direction.[61,62] These features have also been seen in inkjet-printed graphene networks[26] and were present for all AgNW networks produced in this work.

The measured transmittance can be transformed to absorbance, A, using $T = 10^{-A}$. The absorbance is of interest as we expect it to be proportional to the local network thickness[26] and therefore a metric for network uniformity. Shown in Figure 2B is a plot of the local absorbance as a function of the horizontal position (x) along the red dashed line in Figure 2A. This profile is clearly boxlike with a baseline of ∼0.1, corresponding to the absorbance of the PET substrate. The printed line rises from edge to maximum thickness over 300−400 μm and is relatively uniform over the central 1.8 mm. By subtracting the PET absorbance, it is possible to transform the data in Figure 2B to represent the AgNW network transmittance as shown in Figure 2C. This plot shows the mean visible transmittance of the N = 20 line to be ∼50%. Shown in Figure 2D,E are cross-section data for measured absorbance and AgNW network transmittance along the vertical blue dashed line in Figure 2A. These data are similar to the central portion of the lines shown in Figure 2B,C, although the data do appear noisier. However, closer examination (insets) shows the excess noise to be largely due to the striations shown in Figure 2A. The inset data show the thickness variation due to the striations to be at most 25% of the mean thickness.

We can examine the uniformity of the networks directly by extracting data for the network absorbance (i.e., the measured absorbance minus the PET absorbance) for a large number of pixels in the regions marked by the red and blue boxes in Figure 2A. The blue box represents a region 30 μm wide by 12 mm deep (9990 pixels), while the red box represents a region 1.5 mm wide by 30 μm deep (1255 pixels). These data have been plotted as histograms in Figure 2 F,G for the red and blue boxes, respectively. These histograms represent the distributions in local absorbance, and therefore network thicknesses, in the horizontal and vertical directions, respectively. In both cases they are relatively narrow, indicating the lines to be reasonably uniform. However, the distribution in Figure 2G is clearly

DOI: 10.1021/acsami.5b01875
ACS Appl. Mater. Interfaces 2015, 7, 9254−9261

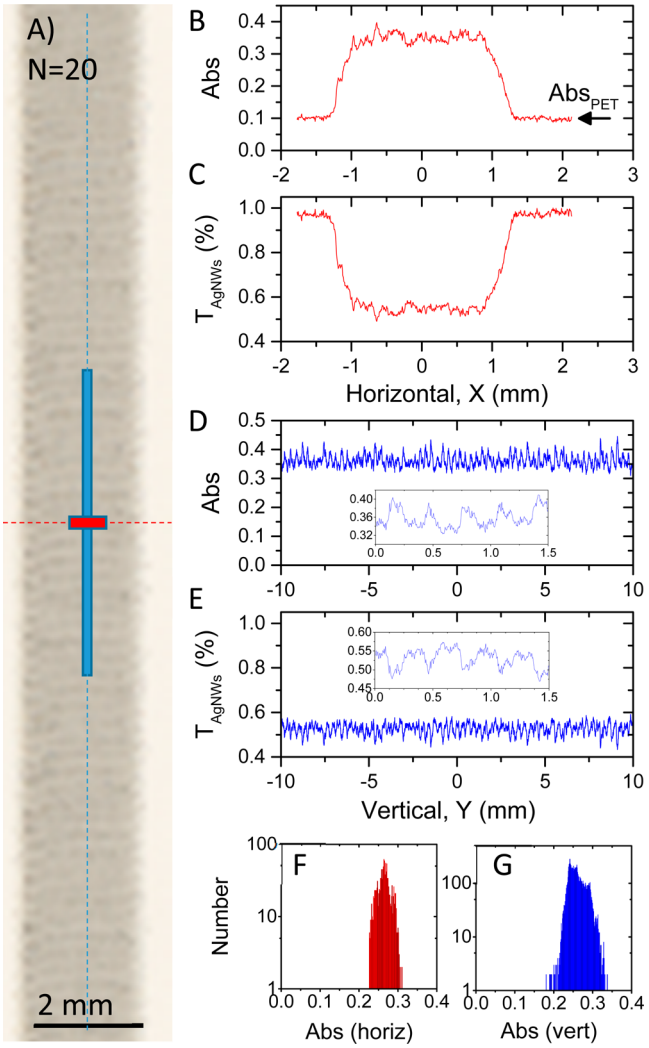

Figure 2. (A) Transmission scanned image of an inkjet-printed (N = 20, w = 2 mm) AgNW line on PET. The print raster direction was horizontal. Note the striations parallel to the raster direction. (B) Measured absorbance profile (extracted from the transmission scan) along a horizontal cross-section (red dashed line in (A)). Note that the absorbance does not fall to zero beyond the edge of the line as the PET substrate was not fully transparent but displayed $A_{PET} \approx 0.1$ ($T_{PET} \approx 80\%$). (C) Transmittance of the AgNW network (extracted from (B) by subtracting the PET absorbance) along a horizontal cross-section. (D, E) Measured absorbance (D) along a vertical cross-section (blue dashed line in (A)) along with the derived AgNW network transmittance (E). The insets in (D) and (E) show variations in both absorbance and transmittance along the vertical cross-section associated with the striations seen in (A). These striations appear with a frequency of 3.1 striations/mm. (F, G) Histograms of AgNW network absorbances (i.e., measured absorbance minus PET absorbance) extracted from regions of the image in (A) schematically shown by the red (F) and blue (G) rectangles.

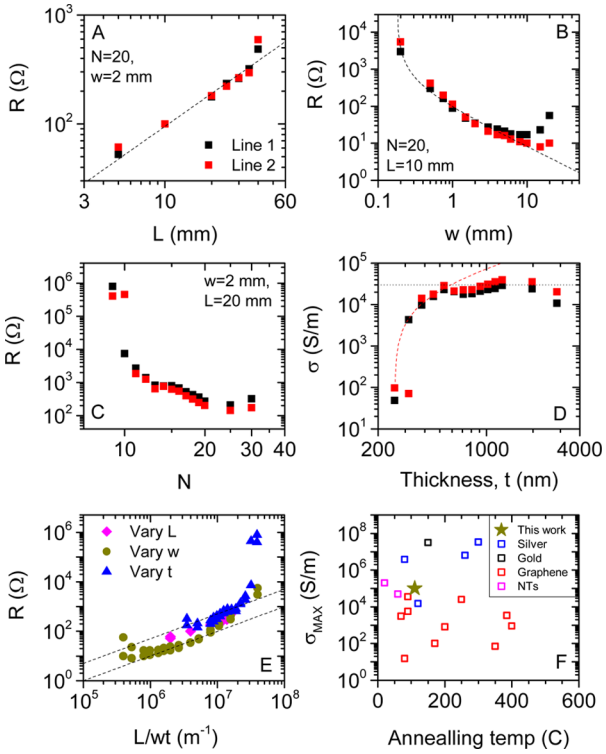

Figure 3. Electrical properties of inkjet-printed silver nanowire networks. (A–C) Electrical resistance of lines of inkjet-printed nanowires plotted as a function of the (A) line length (interelectrode distance), (B) line width, and (C) number of print passes. In (A) the dashed line represents linearity and is consistent with R_s = 19 Ω/□, while in (B) the dashed line represents a fit to eq 2 with R_s = 8 Ω/□ and Δw = 180 μm. (D) Electrical conductivity plotted as a function of the line thickness. The dashed line illustrates percolative behavior, while the dotted line illustrates bulklike behavior. (E) Electrical resistance plotted versus L/wt, were t is calculated from N using eq 1. In this plot a bulklike material obeying Ohm's law will display linear behavior as indicated by the dashed lines (consistent with $\sigma = 2 \times 10^4$ S/m and $\sigma = 10^5$ S/m for the upper and lower curves, respectively). In (A)–(E) data are given for two independent sets of lines. (F) Comparison with literature data. Conductivity plotted versus annealing temperature for lines printed from graphene, carbon nanotube, and silver and gold nanoparticle based inks.

slightly broader due to the presence of the horizontal striations shown in Figure 2A. Statistical analysis shows the ratio of the distribution standard deviation to the mean to be <10% for both distributions.

2.3. Electrical Properties of Silver Nanowire Networks. It is very important that these networks show reasonable electrical properties. To test this, we printed three sets of silver nanowire traces, independently varying the length, L, the width, w, and the number of passes, N. Shown in Figure 3A are data for the resistance as a function of the trace length (N = 20, w = 2 mm) for two independent sets of lines. The resistance scales linearly with the length up to L = 40 mm in a manner consistent with a sheet resistance of R_s = 19 Ω/□ (dashed line). For longer traces the resistance is higher than one would expect. We associate this with the flooding described above which was observed to occur for long traces. Such flooding causes nanowires to bleed out of the traces, leading to significant nonuniformity and reduced electrical performance. We also measured the resistance as a function of the trace width, w, as shown in Figure 3B for two independent sets of lines. From Ohm's law, one would expect the resistance to scale inversely with the width. However, these data deviate considerably from the expected behavior, showing linear behavior only in a narrow range between 1 and 10 mm. For widths above 10 mm, the resistance is higher than expected. This can be explained by solvent flooding and the resultant nonuniformities. The resistances at widths below 1 mm are also higher than expected for an Ohmic material. We associate this phenomenon with line-edge roughness. We assume the traces

DOI: 10.1021/acsami.5b01875
ACS Appl. Mater. Interfaces 2015, 7, 9254–9261

have a minimum width, w_0, and roughness on either side of the trace with amplitude Δw. Then the overall average width is $w = w_0 + \Delta w$, which is equal to the perceived width. However, the width which limits the electrical conductivity is w_0. This means that the most appropriate expression for the line resistance is

$$R = \frac{R_s L}{w_0} = \frac{R_s L}{w - \Delta w} \quad (2)$$

We have fit this expression to the data for $w < 10$ mm, finding very good agreement for $R_s = 8\ \Omega/\square$ and $\Delta w = 180\ \mu$m. Optical microscopy (not shown) confirms the roughness of the line edges to be on the order of hundreds of micrometers, consistent with the data in Figure 2A.

As described above, the thickness of the network is controlled by the number of print passes, N. Shown in Figure 3C is a graph of the measured resistance as a function of N for two independent sets of lines ($L = 20$ mm, $w = 2$ mm). These data show a very high resistance for thin lines, corresponding to a low number of passes. The resistance appears to saturate somewhat for $N > 20$. To understand these data, it is necessary to convert N into thickness, t, using eq 1 and then resistance into conductivity using

$$\sigma = \frac{L}{Rwt} \quad (3)$$

The resulting conductivity data are plotted versus network thickness in Figure 3D. These data clearly show two regimes, one for $t > 500$ nm where conductivity is invariant with thickness and one for $t < 500$ nm where conductivity falls sharply with decreasing thickness. These data are consistent with a number of previous observations relating to the electrical conductivity of nanostructure networks. It is well-known that, for networks of nanoconductors such as silver nanowires, no conductivity is observed below a critical network thickness which is known as the percolation threshold.[63] This threshold corresponds to the formation of the first conductive path. Above the percolation threshold, t_c, the electrical conductivity scales with the thickness as[63]

$$\sigma \propto (t - t_c)^n \quad (4)$$

where n is the percolation exponent. We fit this equation to the data in the thickness range between 250 and 500 nm, finding good agreement using the fit constants $t_c = 255$ nm and $n = 1.1$. While this value of n is close to that expected for two-dimensional networks (i.e., $n = 1.3$),[63] this value of t_c is unexpectedly high as we shall discuss below. It is well-known that, above a certain thickness, the electrical properties of nanostructured networks become thickness independent, displaying a bulklike conductivity.[64,65] This behavior can be seen in Figure 3D for thicknesses greater than 500 mm. In this case the data are consistent with the bulklike conductivity of 3×10^4 S/m. In addition, there is some evidence for a reduction in conductivity at very high thicknesses due to flooding effects. However, we note that there may be some problems with these data and their interpretation. The percolation threshold is much higher than expected. A previous study has shown the percolation thresholds for silver nanowire networks to be below 100 nm.[48] In addition, the transformation from percolative to bulklike behavior occurs here at 500 nm. In previous work this transformation has been observed to occur at thicknesses roughly 3 times the nanowire diameter.[64,65] Thus, we would expect this transformation to occur for network thicknesses of approximately 150 nm. Taken together, these results suggested either our thicknesses are overestimated or our inkjet-printed nanonetworks are morphologically different from those previously studied. If the first suggestion is true, then the conductivities quoted here are underestimates. Further work is required to clarify this point.

We can test the consistency and reproducibility of the electrical properties of these networks by plotting R versus L/wt (i.e., as per eq 3) for all data on a single plot as shown in Figure 3E. We find the data to be roughly consistent and follow the same trend. For an Ohmic material, such a graph should be purely linear. However, here we only observe linearity over a limited range. This behavior is indicated by the dashed lines which show the network conductivities to vary between $\sigma = 2 \times 10^4$ S/m and $\sigma = 10^5$ S/m in the Ohmic (bulklike) regime. These conductivities are relatively low for silver nanowire networks. For example, in our laboratory we have routinely prepared nanowire networks by both spraying and vacuum filtration with conductivities as high as 5×10^6 S/m.[48,49] Other authors have produced even more conductive networks.[50,66] Part of the reason for the low observed conductivity is associated with the reduced length of the wires. The conductivity of nanowire networks is known to scale at least linearly[67] with the nanowire length, with some reports suggesting superlinear behavior.[68] In most cases in the literature, the mean wire length exceeds 5 μm and may be as high as many tens of micrometers,[69] far greater than the mean length of 2.2 μm used here. In addition, as described above, the conductivity of our networks may be somewhat underestimated due to uncertainties in the network thickness. However, it may be that the conductivity of inkjet-printed nanowire networks is lower than that of networks produced by other means due to morphological differences. For example, work in our laboratory has shown that inkjet-printed networks of graphene nanosheets display conductivity about 10 times lower than that of networks produced by vacuum filtration.[26] Further work is required to identify if the inkjet-printed network morphology results in reduced conductivities, perhaps due to disruption of junction annealing. Finally, it is worth noting that the deviations from linearity for both low and high values of L/wt are due to flooding/bleeding and the effect of percolation/line-edge roughness, respectively.

It is important to put these results in context. For printed electronics applications, it would be critically important to print features with high conductivity while minimizing the processing temperature. Shown in Figure 3F is a reasonable, but not exhaustive, attempt to summarize data from the literature by plotting the maximum conductivity achieved versus the maximum annealing temperature used. We have limited data to inkjet-printed structures and categorized in terms of the materials used: graphene,[16−26] nanotubes,[13,40] and nanoparticles of silver[10,41−44] and gold.[45] We find the majority of inks demonstrate lower conductivity and/or higher processing temperatures than those reported here. From this cohort, only two inks, fabricated from nanotubes[40] and silver nanoparticles,[43] show higher conductivity coupled with lower processing temperatures. However, we are certain the conductivity of the printed nanowire networks reported here can be improved significantly by optimizing the thermal annealing process or, for example, by optical welding of junctions.[70]

Finally, we note that, for transparent conductor applications, what is important is not the electrical conductivity but the ratio

DOI: 10.1021/acsami.5b01875
ACS Appl. Mater. Interfaces 2015, 7, 9254−9261

of electrical to optical conductivity,[64] σ_{dc}/σ_{Op} (the optical conductivity is a measure of how strongly a material absorbs light and is proportional to the absorption coefficient). This parameter controls the relationship between transmittance and sheet resistance via

$$T = \left(1 + \frac{Z_0}{2R_s}\frac{\sigma_{Op}}{\sigma_{dc}}\right)^{-2} \quad (5)$$

where Z_0 = 377 Ω is the impedance of free space.[64] According to Figures 2 and 3, for the N = 20 print pass networks, the mean sheet resistance is ∼10 Ω/□ while the transmittance estimated from the scanner is ∼50%. Using eq 5, this means the networks produced here are described by $\sigma_{dc}/\sigma_{Op} \approx 40$. Again using eq 5, we can predict that such networks would display $R_s \approx 90$ Ω/□ at a thickness suitable to give T = 90%. This sort of performance is reasonably good for nanostructured transparent conductors in general[64] but relatively poor for transparent nanowire networks which can display $\sigma_{dc}/\sigma_{Op} > 400$ (ref 64) and $R_s(T{=}90\%) < 10$ Ω/□.[50] The dc to optical conductivity ratio is low primarily because of the low dc conductivity of these networks ($(2-10) \times 10^4$ S/m). To test this, we estimate the optical conductivity (using σ_{dc}/σ_{Op}) to be σ_{Op} = 500−2500 S/m, which is relatively close to but somewhat below the range previously reported, 3800−6500 S/cm.[48,49] Because σ_{Op} is lower than expected, the low value of σ_{dc}/σ_{Op} must be due to the relatively low value of σ_{dc}. The reasons for this have been described above.

3. CONCLUSION

In summary, we have demonstrated inkjet printing of networks of silver nanowires, from optimized isopropyl alcohol−diethylene glycol dispersions. We have identified the main challenges to achieving this, resolving them one by one. The resultant networks are reasonably uniform and have good electrical properties. The lowest sheet resistance observed was 8 Ω/□, while the highest conductivity was 10^5 S/m. Such optimized performances were achieved for line widths of 1−10 mm and network thicknesses of 0.5−2 μm deposited from ∼10−20 passes while using processing temperatures of no more than 110 °C. While further improvements are necessary, these data are already competitive with most of the published data on printed nanomaterials.

We believe this work is important as one of the first steps toward the ability to print highly conductive, transparent, patterned networks of metallic nanowires. Future work will see the improvement of the network conductivity, perhaps by the introduction of low-temperature sintering processes to weld nanowire junctions together. This will lead to inkjet-printed nanowires becoming an important addition to the palette of materials already available to the printed electronics community.

4. METHODS

Silver nanowires were purchased from Seashell Technology as a suspension in isopropyl alcohol at a concentration of 5 mg/mL. Ultrasonically induced scission of the silver nanowires to reduce their length was carried out in a low-power sonic bath (Branson 1510E-MT) operating at a frequency of 42 kHz ± 5% and a rated power of 70 W.

In this work, a Dimatix materials printer 2800 was used. This laboratory inkjet printer uses a single printhead having 16 ejection nozzles (nozzle diameter 21.5 μm) spaced 254 μm apart, driven by piezoelectric elements jetting 10 pL droplets, and fed with a solvent-based ink from a fluid bag encased in a plastic housing attached to the printhead. The printhead angle was 4.5°, and a typical drop spacing was 20 μm with a 50% degree of overlap. The drop frequency was 5 kHz, and the jetting waveform parameters are shown in the Supporting Information. We note that clogging of the printhead did not occur if the jetting parameters described above were applied. However, the use of appropriate cleaning cycles was important to avoiding nozzle clogging. It was observed that purging of the printhead and ink tank following use greatly extended the useable life of the printhead. For example, preventing drying of the nanowires on the printhead was particularly important. It was found that, with regular purging during printing and careful cleaning following printing, the printhead could be used for several days, and up to 10 days in some cases, without any degradation in print performance. The substrate used was a coated PET designed for printing of silver inks (Mitsubishi NB-TP-3GU100). Solvent evaporation was managed as described in the text. The inkjet printer used in this study defines patterns based on an xy grid coordinate system. Patterns are programmed as bitmap images. For this work the "length" and "width" were varied independently by changing the pattern shape, drawing a series of adjacent lines with the following variables: constant length (in the y direction) with varied width (in the x direction), constant width (in the x direction) with varied length (in the y direction). The drop volume, frequency, and spacing were held constant throughout.

Profile uniformity analysis of a silver nanowire network after 20 print passes was made using an Epson Perfection V700 photo flatbed transmission scanner with a bit depth of 48-bits per pixel and a spatial resolution of 4800 dpi (see the Supporting Information for more information). Scanning electron microscopy was performed using a Carl Zeiss Ultra Plus scanning electron microscope. The electrical characterization was performed using a Keithley 2400 source meter using the four-probe technique.

■ ASSOCIATED CONTENT

Supporting Information

Detailed description of the printing optimization. This material is available free of charge via the Internet at http://pubs.acs.org.

■ AUTHOR INFORMATION

Corresponding Author

*E-mail: colemaj@tcd.ie.

Notes

The authors declare no competing financial interest.

■ ACKNOWLEDGMENTS

We acknowledge support from the Science Foundation Ireland (SFI)-funded AMBER research center (Grant SFI/12/RC/2278).

■ REFERENCES

(1) Hutchings, I. M.; Martin, G. D. *Inkjet Technology for Digital Fabrication*; John Wiley & Sons: Chichester, West Sussex, U.K., 2013.
(2) Kamyshny, A.; Magdassi, S. Conductive Nanomaterials for Printed Electronics. *Small* **2014**, *10*, 3515−3535.
(3) Yan, H.; Chen, Z. H.; Zheng, Y.; Newman, C.; Quinn, J. R.; Dotz, F.; Kastler, M.; Facchetti, A. A High-Mobility Electron-Transporting Polymer for Printed Transistors. *Nature* **2009**, *457*, 679−U1.
(4) Del Mauro, A. D.; Diana, R.; Grimaldi, I. A.; Loffredo, F.; Morvillo, P.; Villani, F.; Minarini, C. Polymer Solar Cells with Inkjet-Printed Doped-PEDOT: PSS Anode. *Polym. Compos.* **2013**, *34*, 1493−1499.
(5) Crowley, K.; Morrin, A.; Shepherd, R. L.; Panhuis, M. I. H.; Wallace, G. G.; Smyth, M. R.; Killard, A. J. Fabrication of Polyaniline-Based Gas Sensors Using Piezoelectric Inkjet and Screen Printing for the Detection of Hydrogen Sulfide. *IEEE Sens. J.* **2010**, *10*, 1419−1426.

DOI: 10.1021/acsami.5b01875
ACS Appl. Mater. Interfaces 2015, 7, 9254−9261

(6) Mire, C. A.; Agrawal, A.; Wallace, G. G.; Calvert, P.; Panhuis, M. I. H. Inkjet and Extrusion Printing of Conducting Poly(3,4-ethylenedioxythiophene) Tracks on and Embedded in Biopolymer Materials. *J. Mater. Chem.* **2011**, *21*, 2671−2678.
(7) Wood, V.; Panzer, M. J.; Chen, J. L.; Bradley, M. S.; Halpert, J. E.; Bawendi, M. C.; Bulovic, V. Inkjet-Printed Quantum Dot−Polymer Composites for Full-Color AC-Driven Displays. *Adv. Mater.* **2009**, *21*, 2151−2155.
(8) Lee, H. H.; Chou, K. S.; Huang, K. C. Inkjet Printing of Nanosized Silver Colloids. *Nanotechnology* **2005**, *16*, 2436−2441.
(9) Takagi, Y.; Nobusa, Y.; Gocho, S.; Kudou, H.; Yanagi, K.; Kataura, H.; Takenobu, T. Inkjet Printing of Aligned Single-Walled Carbon-Nanotube Thin Films. *Appl. Phys. Lett.* **2013**, *102*, 143107.
(10) Kim, T.; Song, H.; Ha, J.; Kim, S.; Kim, D.; Chung, S.; Lee, J.; Hong, Y. Inkjet-Printed Stretchable Single-Walled Carbon Nanotube Electrodes with Excellent Mechanical Properties. *Appl. Phys. Lett.* **2014**, *104*, 113103.
(11) Sajed, F.; Rutherglen, C. All-Printed and Transparent Single Walled Carbon Nanotube Thin Film Transistor Devices. *Appl. Phys. Lett.* **2013**, *103*, 143303.
(12) Beecher, P.; Servati, P.; Rozhin, A.; Colli, A.; Scardaci, V.; Pisana, S.; Hasan, T.; Flewitt, A. J.; Robertson, J.; Hsieh, G. W.; Li, F. M.; Nathan, A.; Ferrari, A. C.; Milne, W. I. Ink-Jet Printing of Carbon Nanotube Thin Film Transistors. *J. Appl. Phys.* **2007**, *102*, 025005.
(13) Song, J.-W.; Kim, J.; Yoon, Y.-H.; Choi, B.-S.; Kim, J.-H.; Han, C.-S. Inkjet Printing of Single-Walled Carbon Nanotubes and Electrical Characterization of the Line Pattern. *Nanotechnology* **2008**, *19*, 095702.
(14) Shimoni, A.; Azoubel, S.; Magdassi, S. Inkjet Printing of Flexible High-Performance Carbon Nanotube Transparent Conductive Films by "Coffee Ring Effect". *Nanoscale* **2014**, *6*, 11084−11488.
(15) Small, W. R.; Panhuis, M. I. H. Inkjet Printing of Transparent, Electrically Conducting Single-Walled Carbon-Nanotube Composites. *Small* **2007**, *3*, 1500−1503.
(16) Dua, V.; Surwade, S. P.; Ammu, S.; Agnihotra, S. R.; Jain, S.; Roberts, K. E.; Park, S.; Ruoff, R. S.; Manohar, S. K. All-Organic Vapor Sensor Using Inkjet-Printed Reduced Graphene Oxide. *Angew. Chem., Int. Ed.* **2010**, *49*, 2154−2157.
(17) Huang, L.; Huang, Y.; Liang, J. J.; Wan, X. J.; Chen, Y. S. Graphene-Based Conducting Inks for Direct Inkjet Printing of Flexible Conductive Patterns and Their Applications in Electric Circuits and Chemical Sensors. *Nano Res.* **2011**, *4*, 675−684.
(18) Kong, D.; Le, L. T.; Li, Y.; Zunino, J. L.; Lee, W. Temperature-Dependent Electrical Properties of Graphene Inkjet-Printed on Flexible Materials. *Langmuir* **2012**, *28*, 13467−13472.
(19) Le, L. T.; Ervin, M. H.; Qiu, H. W.; Fuchs, B. E.; Lee, W. Y. Graphene Supercapacitor Electrodes Fabricated by Inkjet Printing and Thermal Reduction of Graphene Oxide. *Electrochem. Commun.* **2011**, *13*, 355−358.
(20) Li, J.; Ye, F.; Vaziri, S.; Muhammed, M.; Lemme, M. C.; Ostling, M. Efficient Inkjet Printing of Graphene. *Adv. Mater.* **2013**, *25*, 3985−3992.
(21) Lim, S.; Kang, B.; Kwak, D.; Lee, W. H.; Lim, J. A.; Cho, K. Inkjet-Printed Reduced Graphene Oxide/Poly(vinyl alcohol) Composite Electrodes for Flexible Transparent Organic Field-Effect Transistors. *J. Phys. Chem. C* **2012**, *116*, 7520−7525.
(22) Secor, E. B.; Prabhumirashi, P. L.; Puntambekar, K.; Geier, M. L.; Hersam, M. C. Inkjet Printing of High Conductivity, Flexible Graphene Patterns. *J. Phys. Chem. Lett.* **2013**, *4*, 1347−1351.
(23) Shin, K. Y.; Hong, J. Y.; Jang, J. Micropatterning of Graphene Sheets by Inkjet Printing and Its Wideband Dipole-Antenna Application. *Adv. Mater.* **2011**, *23*, 2113−2118.
(24) Shin, K. Y.; Hong, J. Y.; Jang, J. Flexible and Transparent Graphene Films as Acoustic Actuator Electrodes Using Inkjet Printing. *Chem. Commun.* **2011**, *47*, 8527−8529.
(25) Torrisi, F.; Hasan, T.; Wu, W. P.; Sun, Z. P.; Lombardo, A.; Kulmala, T. S.; Hsieh, G. W.; Jung, S. J.; Bonaccorso, F.; Paul, P. J.; Chu, D. P.; Ferrari, A. C. Inkjet-Printed Graphene Electronics. *ACS Nano* **2012**, *6*, 2992−3006.
(26) Finn, D. J.; Lotya, M.; Cunningham, G.; Smith, R. J.; McCloskey, D.; Donegan, J. F.; Coleman, J. N. Inkjet Deposition of Liquid-Exfoliated Graphene and MoS_2 Nanosheets for Printed Device Applications. *J. Mater. Chem. C* **2014**, *2*, 925−932.
(27) Torrisi, F.; Coleman, J. N. Electrifying Inks with 2D Materials. *Nat. Nanotechnol.* **2014**, *9*, 738−739.
(28) Yao, Y.; Tolentino, L.; Yang, Z.; Song, X.; Zhang, W.; Chen, Y.; Wong, C.-P. High-Concentration Aqueous Dispersions of MoS_2. *Adv. Funct. Mater.* **2013**, *23*, 3577−3583.
(29) Zheng, J.; Zhang, H.; Dong, S.; Liu, Y.; Nai, C. T.; Shin, H. S.; Jeong, H. Y.; Liu, B.; Loh, K. P. High Yield Exfoliation of Two-Dimensional Chalcogenides Using Sodium Naphthalenide. *Nat. Commun.* **2014**, *5*, 2995.
(30) Li, J.; Naiini, M. M.; Vaziri, S.; Lemme, M. C.; Östling, M. Inkjet Printing of MoS_2. *Adv. Funct. Mater.* **2014**, *24*, 6524−6531.
(31) Sirringhaus, H.; Kawase, T.; Friend, R. H.; Shimoda, T.; Inbasekaran, M.; Wu, W.; Woo, E. P. High-Resolution Inkjet Printing of All-Polymer Transistor Circuits. *Science* **2000**, *290*, 2123−2126.
(32) Zhang, J.; Zhao, Y.; Wei, Z. M.; Sun, Y. M.; He, Y. D.; Di, C. A.; Xu, W.; Hu, W. P.; Liu, Y. Q.; Zhu, D. B. Inkjet-Printed Organic Electrodes for Bottom-Contact Organic Field-Effect Transistors. *Adv. Funct. Mater.* **2011**, *21*, 786−791.
(33) Karuwan, C.; Sriprachuabwong, C.; Wisitsoraat, A.; Phokharatkul, D.; Sritongkham, P.; Tuantranont, A. Inkjet-Printed Graphene-Poly(3,4-ethylenedioxythiophene):Poly(styrene-sulfonate) Modified on Screen Printed Carbon Electrode for Electrochemical Sensing of Salbutamol. *Sens. Actuators, B* **2012**, *161*, 549−555.
(34) Monereo, O.; Claramunt, S.; de Marigorta, M. M.; Boix, M.; Leghrib, R.; Prades, J. D.; Cornet, A.; Merino, P.; Merino, C.; Cirera, A. Flexible Sensor Based on Carbon Nanofibers with Multifunctional Sensing Features. *Talanta* **2013**, *107*, 239−247.
(35) Bharathan, J.; Yang, Y. Polymer Electroluminescent Devices Processed by Inkjet Printing: I. Polymer Light-Emitting Logo. *Appl. Phys. Lett.* **1998**, *72*, 2660−2662.
(36) Chen, P. C.; Chen, H. T.; Qiu, J.; Zhou, C. W. Inkjet Printing of Single-Walled Carbon Nanotube/RuO_2 Nanowire Supercapacitors on Cloth Fabrics and Flexible Substrates. *Nano Res.* **2010**, *3*, 594−603.
(37) Kossyrev, P. Carbon Black Supercapacitors Employing Thin Electrodes. *J. Power Sources* **2012**, *201*, 347−352.
(38) Hoth, C. N.; Schilinsky, P.; Choulis, S. A.; Brabec, C. J. Printing Highly Efficient Organic Solar Cells. *Nano Lett.* **2008**, *8*, 2806−2813.
(39) Kang, B.; Lee, W. H.; Cho, K. Recent Advances in Organic Transistor Printing Processes. *ACS Appl. Mater. Interfaces* **2013**, *5*, 2302−2315.
(40) Gracia-Espino, E.; Sala, G.; Pino, F.; Halonen, N.; Luomahaara, J.; Mäklin, J.; Tóth, G.; Kordás, K.; Jantunen, H.; Terrones, M.; Helistö, P.; Seppä, H.; Ajayan, P. M.; Vajtai, R. Electrical Transport and Field-Effect Transistors Using Inkjet-Printed SWCNT Films Having Different Functional Side Groups. *ACS Nano* **2010**, *4*, 3318−3324.
(41) Faddoul, R.; Reverdy-Bruas, N.; Blayo, A.; Khelifi, B. Inkjet Printing of Silver Nano-Suspensions on Ceramic Substrates—Sintering Temperature Effect on Electrical Properties. *Microelectron. Eng.* **2013**, *105*, 31−39.
(42) Hsien-Hsueh, L.; Kan-Sen, C.; Kuo-Cheng, H. Inkjet Printing of Nanosized Silver Colloids. *Nanotechnology* **2005**, *16*, 2436.
(43) Perelaer, J.; de laat, A. W. M.; Hendriks, C. E.; Schubert, U. S. Inkjet-Printed Silver Tracks: Low Temperature Curing and Thermal Stability Investigation. *J. Mater. Chem.* **2008**, *18*, 3209−3215.
(44) Polzinger, B.; Schoen, F.; Matic, V.; Keck, J.; Willeck, H.; Eberhardt, W.; Kueck, H. UV-Sintering of Inkjet-Printed Conductive Silver Tracks. *Nanotechnology (IEEE-NANO), 2011 11th IEEE Conference on*, Portland, OR, Aug 15−18, 2011; IEEE: New York, 2011; pp 201−204.
(45) Huang, D.; Liao, F.; Molesa, S.; Redinger, D.; Subramanian, V. Plastic-Compatible Low Resistance Printable Gold Nanoparticle Conductors for Flexible Electronics. *J. Electrochem. Soc.* **2003**, *150*, G412−G417.

DOI: 10.1021/acsami.5b01875
ACS Appl. Mater. Interfaces 2015, 7, 9254−9261

(46) Layani, M.; Kamyshny, A.; Magdassi, S. Transparent Conductors Composed of Nanomaterials. *Nanoscale* **2014**, *6*, 5581−5591.
(47) Langley, D.; Giusti, G.; Mayousse, C.; Celle, C.; Bellet, D.; Simonato, J. P. Flexible Transparent Conductive Materials Based on Silver Nanowire Networks: A Review. *Nanotechnology* **2013**, *24*, 452001.
(48) De, S.; Higgins, T.; Lyons, P. E.; Doherty, E. M.; Nirmalraj, P. N.; Blau, W. J.; Boland, J. J.; Coleman, J. N. Silver Nanowire Networks as Flexible, Transparent, Conducting Films: Extremely High DC to Optical Conductivity Ratios. *ACS Nano* **2009**, *3*, 1767−1774.
(49) Scardaci, V.; Coull, R.; Lyons, P. E.; Rickard, D.; Coleman, J. N. Spray Deposition of Highly Transparent, Low-Resistance Networks of Silver Nanowires over Large Areas. *Small* **2011**, *7*, 2621−2628.
(50) Lee, S. J.; Kim, Y.-H.; Kim, J. K.; Baik, H.; Park, J. H.; Lee, J.; Nam, J.; Park, J. H.; Lee, T.-W.; Yi, G.-R.; Cho, J. H. A Roll-to-Roll Welding Process for Planarized Silver Nanowire Electrodes. *Nanoscale* **2014**, *6*, 11828−34.
(51) Hu, L.; Kim, H. S.; Lee, J.-Y.; Peumans, P.; Cui, Y. Scalable Coating and Properties of Transparent, Flexible, Silver Nanowire Electrodes. *ACS Nano* **2010**, *4*, 2955−2963.
(52) Lee, J. Y.; Connor, S. T.; Cui, Y.; Peumans, P. Solution-Processed Metal Nanowire Mesh Transparent Electrodes. *Nano Lett.* **2008**, *8*, 689−692.
(53) Madaria, A. R.; Kumar, A.; Ishikawa, F. N.; Zhou, C. W. Uniform, Highly Conductive, and Patterned Transparent Films of a Percolating Silver Nanowire Network on Rigid and Flexible Substrates Using a Dry Transfer Technique. *Nano Res.* **2010**, *3*, 564−573.
(54) Sorel, S.; Bellet, D.; Coleman, J. N. Relationship between Material Properties and Transparent Heater Performance for Both Bulk-like and Percolative Nanostructured Networks. *ACS Nano* **2014**, *8*, 4805−4814.
(55) Sepulveda-Mora, S. B.; Cloutier, S. G. Figures of Merit for High-Performance Transparent Electrodes Using Dip-Coated Silver Nanowire Networks. *J. Nanomater.* **2012**, *2012*, 286104.
(56) Gysling, H. J. Nanoinks in Inkjet Metallization—Evolution of Simple Additive-Type Metal Patterning. *Curr. Opin. Colloid Interface Sci.* **2014**, *19*, 155−162.
(57) Wu, J.-T.; Hsu, S. L.-C.; Tsai, M.-H.; Liu, Y.-F.; Hwang, W.-S. Direct Ink-Jet Printing of Silver Nitrate-Silver Nanowire Hybrid Inks To Fabricate Silver Conductive Lines. *J. Mater. Chem.* **2012**, *22*, 15599−15605.
(58) Lu, H.; Lin, J.; Wu, N.; Nie, S.; Luo, Q.; Ma, C.-Q.; Cui, Z. Inkjet Printed Silver Nanowire Network as Top Electrode for Semi-Transparent Organic Photovoltaic Devices. *Appl. Phys. Lett.* **2015**, *106*, 093302.
(59) Stegen, J. Mechanics of Carbon Nanotube Scission under Sonication. *J. Chem. Phys.* **2014**, *140*, 244908.
(60) Derby, B.; Reis, N. Inkjet Printing of Highly Loaded Particulate Suspensions. *MRS Bull.* **2003**, *28*, 815−818.
(61) Lyon, P. J.; Carter, J.; Creighton, C.; Gregory, H. Solvents for PEDOT-Solutions for Ink-Jet Printing. U.S. Patent US 8431040 B2, 2009.
(62) Castano, J.; Girones, X. Method of Reducing Vertical Banding in Ink Jet Printing. U.S. Patent US 6595621 B2, 2003.
(63) Stauffer, D. S.; Aharony, A. *Introduction to Percolation Theory*; Taylor and Francis: London, 1994.
(64) De, S.; Coleman, J. N. The Effects of Percolation in Nanostructured Transparent Conductors. *MRS Bull.* **2011**, *36*, 774−781.
(65) De, S.; King, P. J.; Lyons, P. E.; Khan, U.; Coleman, J. N. Size Effects and the Problem with Percolation in Nanostructured Transparent Conductors. *ACS Nano* **2010**, *4*, 7064−7072.
(66) Leem, D.-S.; Edwards, A.; Faist, M.; Nelson, J.; Bradley, D. D. C.; de Mello, J. C. Efficient Organic Solar Cells with Solution-Processed Silver Nanowire Electrodes. *Adv. Mater.* **2011**, *23*, 4371−4375.
(67) Sorel, S.; Lyons, P. E.; De, S.; Dickerson, J. C.; Coleman, J. N. The Dependence of the Optoelectrical Properties of Silver Nanowire Networks on Nanowire Length and Diameter. *Nanotechnology* **2012**, *23*, 185201.
(68) Hecht, D.; Hu, L. B.; Gruner, G., Conductivity Scaling with Bundle Length and Diameter in Single Walled Carbon Nanotube Networks. *Appl. Phys. Lett.* **2006**, *89*.
(69) Lee, P.; Lee, J.; Lee, H.; Yeo, J.; Hong, S.; Nam, K. H.; Lee, D.; Lee, S. S.; Ko, S. H. Highly Stretchable and Highly Conductive Metal Electrode by Very Long Metal Nanowire Percolation Network. *Adv. Mater.* **2012**, *24*, 3326−3332.
(70) Garnett, E. C.; Cai, W.; Cha, J. J.; Mahmood, F.; Connor, S. T.; Christoforo, M. G.; Cui, Y.; McGehee, M. D.; Brongersma, M. L. Self-Limited Plasmonic Welding of Silver Nanowire Junctions. *Nat. Mater.* **2012**, *11*, 241−249.

DOI: 10.1021/acsami.5b01875
ACS Appl. Mater. Interfaces 2015, 7, 9254−9261